Unsaturated Soils: Advances in Geo-Engineering – Toll et al. (eds)
© 2008 Taylor & Francis Group, London, ISBN 978-0-415-47692-8

A multi-cell extension to the Barcelona Basic Model

W.T. Solowski & R.S. Crouch
Durham University, Durham, UK

D. Gallipoli
University of Glasgow, Glasgow, UK

ABSTRACT: One of the sources of discrepancy between laboratory observations and the predicted behaviour of unsaturated soil (by many existing constitutive models) is the sharp transition between the elastic and elasto-plastic regimes exhibited by the latter but not the former. Such a transition is present in, for example, the Barcelona Basic Model. This paper suggests that by using the water retention curve and a multi-cell approach it is possible to overcome this limitation. The proposed enhancement may be incorporated relatively easily into many existing elasto-plastic models for unsaturated soils without addition of any new constitutive variables. The introduction of the algorithm presented here can improve the predictions in pre-yield states. In this paper the multi-cell approach has been implemented into the Barcelona Basic Model (BBM). The algorithm is described in detail using an illustrative stress path that involves hydrostatic compression, drying and wetting. The paper closes with a comparison of the modified model with the original BBM.

1 INTRODUCTION

The Barcelona Basic Model (BBM) proposed by Alonso et al. (1990) is perhaps the most widely used nonlinear continuum constitutive model for unsaturated soils. Despite its attractiveness this model has several shortcomings. For example, the model predicts an abrupt transition from elastic to elasto-plastic behaviour in a similar fashion to the Modified Cam Clay (MCC) model. In the light of laboratory evidence, such a response simplifies the behaviour of unsaturated soil substantially. To rectify this issue, the commonly employed solution is to create a constitutive model within a multi- or bounding surface plasticity framework (e.g. Russell & Khalili, 2005). Unfortunately, such an approach leads to (i) an increase in number of constants required by the model and (ii) additional numerical complexity. Therefore multi- or bounding surface plasticity models require greater experience to calibrate when compared with conventional elasto-plastic models.

The proposed modifications to the BBM allow for a smoother modelling of the transition between the elastic and elasto-plastic regimes. The modified model uses only the BBM constants with the additional information given by the water retention curve. Also, the numerical algorithms required remain mostly the same as for the original BBM. The calibration process of the modified model is, however, more involved, but this is not a serious limitation.

2 UNSATURATED SOIL MICROSTRUCTURE

The main idea of the proposed constitutive model stems from an examination of the microstructure and water retention in unsaturated soils. Most constitutive models (with the exception of models using a double structure framework, such as developed by Gens & Alonso, 1992) ignore important aspects of microscopic soil fabric and thus assume a homogeneous medium, simply extending the continuum constitutive frameworks developed for fully saturated soils. However, fine grained unsaturated soil can have a much more complex fabric at microscopic level than saturated soil. The clay platelets combine together creating larger clusters commonly referred to as aggregates (this fact has been pointed out already by Alonso et al., 1987). The pores between the aggregates (macropores) are larger than within the aggregates (micropores) which leads to a double porosity structure. Such a structure can be seen in environmental scanning electron microscopy (ESEM) images and is confirmed by mercury intrusion porosimetry (MIP) tests (see e.g. Monroy, 2005).

The non-homogeneous microstructure of unsaturated soil is also indirectly confirmed by the water retention curve. This curve describes the relationship between the suction and the water content for a given soil. The amount of water retained under a given suction is related to pore size distribution of the soil according to the Young-Laplace equation. Therefore,

the water retention curve can be used to calculate the radius of the largest pores filled with water at a given suction. As the water content of soil is known, the volume of pores with a smaller radius than this can also be estimated.

Such an estimation of pore sizes in unsaturated soil via the water retention curve is helpful but imperfect, as drying/wetting of the soil leads to changes in its structure. The soil structure (skeleton) may change irreversibly as the wet portion of soil is drawn together or undergoes swelling due to variation of suction. So, while the water retention curve can be used to estimate the pore size distribution, the outcome will not be entirely representative for the soil given the non-uniqueness of the relationship between suction and water content caused by both irreversible strains and hydraulic hysteresis. This dependence of water retention behaviour on the soil deformation history has indeed been observed during experiments and partially incorporated in recent models for water retention behaviour (Gallipoli et al., 2003).

3 USING WATER RETENTION CURVE TO ENHANCE THE CONSTITUTIVE MODEL

Despite the shortcomings mentioned above, the water retention curve carries useful information about the microstructural behaviour of unsaturated soil. It is thus appropriate to use this information in constitutive modelling. Here, to keep the modification as simple as possible, it is assumed that a unique water retention curve, independent from the deformation and wetting/drying history of soil, exists.

Such a water retention curve can be expressed as a direct relationship between suction and degree of saturation. Given this relationship, it is straightforward to determine what percentage of soil has experienced a maximum given value of suction—it is the corresponding value of degree of saturation S_r read from the water retention curve. It follows that at a given value of suction, the average mean stress acting on the soil skeleton is equal to the sum of the external stress p and the current suction multiplied by the corresponding degree of saturation sS_r. This follows from the stress definition given by Houlsby (1997).

Such an average stress does not account, however, for the history of soil, i. e. it does not take into account that the parts of soil which are currently dry, previously experienced suction. An assumption has been made here that the dried part of soil behaves 'as though' the suction value that it has recently experienced is still acting.

The soil then may be thought of as being composed of a large number of internal cells. In S_r percent of cells the suction is equal to the current suction s. It is assumed that in each of the remaining cells the amount of suction acting is equal to the latest value of suction experienced in that cell. Then, for every cell a separate instance of the constitutive model is run. During the analysis each cell experiences the same mean stress, but has a separate hardening parameter value and suction. After the computations, the deformations are averaged. During implementation, the number of cells, n, must be chosen to arrive at a balance between computational efficiency and realism.

4 IMPLEMENTATION OF MULTI-CELL FRAMEWORK FOR BBM

The multi-cell concept based on the use of the water retention curve as described above has been implemented in the BBM.

It is convenient to assume that in the initial state the material is saturated, so that the initial value of suction in all cells is set equal to zero. The other assumption made at the beginning of the simulation is that the hardening parameter p_0^* (BBM preconsolidation stress for saturated conditions) in all cells is identical. Once suction is applied, the values of current preconsolidation pressure p_0 in each cell are dependent on the value of hardening parameter p_0^* and the most recently experienced suction s

$$p_0 = p_0(p_0^*, s) = p^c \left(\frac{p_0^*}{p^c}\right)^{\frac{\lambda(0)-\kappa}{\lambda(s)-\kappa}} \tag{1}$$

where p^c is the value of the reference stress and $\lambda(s)$ is the slope of the virgin compression line at suction s. This slope is calculated as:

$$\lambda(s) = \lambda(0)\left[(1-r)e^{-\beta s} + r\right] \tag{2}$$

where $\lambda(0)$is the slope of the virgin compression line for the fully saturated soil, r and β are BBM constants. In every cell a separate instance of the BBM is used and, subsequently, the values from all cells are averaged.

5 EXAMPLE

In this section an illustrative example is given. To keep the example as simple as possible it was decided to use 5 cells (n = 5). The water retention curve is given in Figure 2. Initially (Fig. 1, point A) the soil is fully saturated, with a mean net stress p of 10 kPa which is also the value used for the reference pressure p^c in BBM. The soil is normally consolidated, so the hardening parameter p_0^* is equal to 10 kPa. The other BBM parameters used were: elastic stiffness parameter for changes in net mean stress $\kappa = 0.02$, elastic

stiffness parameter for changes in suction $\kappa_s = 0.05$, atmospherics pressure $p_{atm} = 100$ kPa, stiffness parameter for changes in net mean stress for virgin states of the soil (with suction $s = 0$) $\lambda(0) = 0.2$, parameter defining the maximum increase of soil stiffness with suction $\beta = 0.01$ 1/kPa and parameter defining the maximum soil stiffness r = 0.75. The initial specific volume at the reference pressure p^c is set to 2.6. The initial soil state is given in Table 1.

The stress path and corresponding values of the specific volume of soil are summarised in Figure 1. First, the soil is isotropic loaded until $p = 100$ kPa (Fig. 1, path A-B). The state of soil after such loading is given in Table 2.

At this stage (Fig. 1, point B) the values of specific volume for each cell v_1^i in Table 2 are equal and calculated as

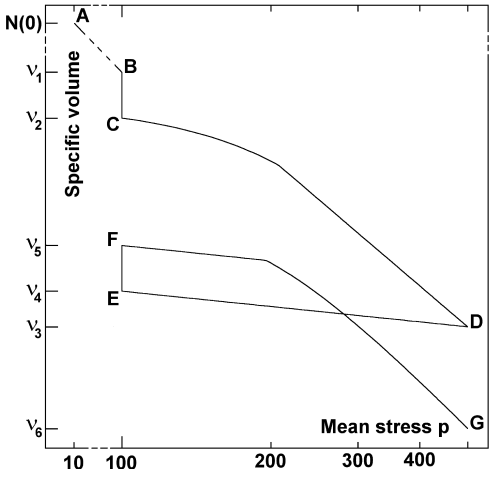

Figure 1. Stress path, as calculated in the example.

Table 1. Initial condition of soil (Fig. 1, point A).

Cell (i)	1	2	3	4	5
Hard. par. p_0^*[kPa]	10	10	10	10	10
Suction [kPa]	0	0	0	0	0
Specific vol. $N(0)$*	2.6	2.6	2.6	2.6	2.6

*$N(0)$ is the specific volume at the reference pressure p^c.

Table 2. Soil state at $p = 100$ kPa (Fig. 1, point B).

Cell (i)	1	2	3	4	5
Hard. par. p_0^*[kPa]	100	100	100	100	100
Suction [kPa]	0	0	0	0	0
Specific volume v_1^i	2.139	2.139	2.139	2.139	2.139

$$v_1^i = N(0) - \lambda(0) \ln \frac{p_0^{*,i}}{p^c}, \quad i = 1..5 \tag{3}$$

The average specific volume is

$$v_1 = \frac{1}{n} \sum_{i=1}^{n} v_1^i = \frac{v_1^1 + v_1^2 + v_1^3 + v_1^4 + v_1^5}{5} = 2.139 \tag{4}$$

where n is the number of cells used.

The soil is then dried until suction reaches 200 kPa (Fig 1, B–C). The values of suction corresponding to S_r equal to 0.9, 0.7, 0.5 and 0.47 are 30 kPa, 100 kPa, 180 kPa and 200 kPa respectively (see Fig. 2). The cells are dried in a sequence, assuming that the cell is dry when it is less then half full. This fully arbitrary assumption leads to drying the cells once the degree of saturation reaches 0.9, 0.7, 0.5, 0.3 which correspond to 30 kPa, 100 kPa, 180 kPa and 460 kPa suction respectively (see Fig. 2). As at final suction 200 kPa the corresponding degree of saturation is $0.47 > 0.3$, so the cells 4 & 5 remain wet. The evolution of cell suction is given by Table 3, where $s(S_r)$ denotes suction corresponding to the value of degree of saturation as given by the water retention curve (Figs 2 & 3).

The soil state after drying is summarized in Table 4. The specific volume for each cell v_2^i and preconsolidation pressure p_0^i in Table 4 are calculated using:

$$v_2^i = v_1^i - \kappa_s \ln \frac{s^i + p_{\text{atm}}}{p_{\text{atm}}}, \quad i = 1..5 \tag{5}$$

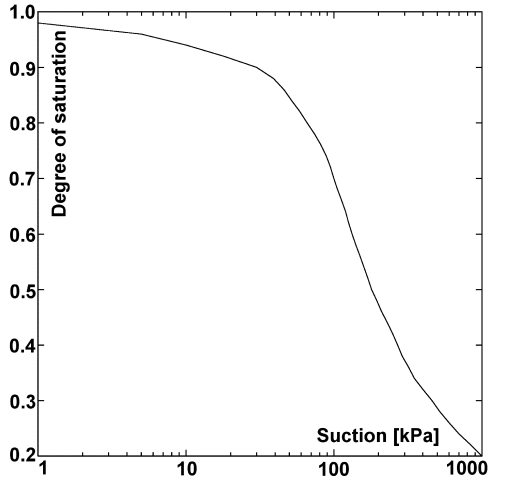

Figure 2. Water retention curve.

Table 3. Evolution of suction during drying.

	Suction Value [kPa]				
Cell (i)	1	2	3	4	5
$S_r > 0.9$	$s(S_r)$	$s(S_r)$	$s(S_r)$	$s(S_r)$	$s(S_r)$
$S_r = 0.9$	30	30	30	30	30
$0.9 > S_r > 0.7$	30	$s(S_r)$	$s(S_r)$	$s(S_r)$	$s(S_r)$
$Sr = 0.7$	30	100	100	100	100
$0.7 > S_r > 0.5$	30	100	$s(S_r)$	$s(S_r)$	$s(S_r)$
$S_r = 0.5$	30	100	180	180	180
$0.5 > S_r > 0.3$	30	100	180	$s(S_r)$	$s(S_r)$
$S_r = 0.47$	30	100	180	200	200

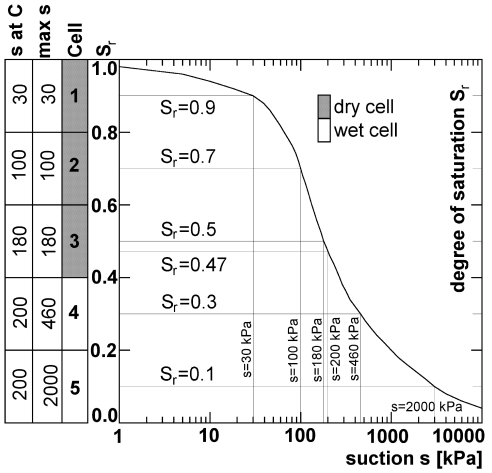

Figure 3. Illustration of suction distribution within cells after drying to $s = 200$ kPa (Fig. 1, point C). A cell is assumed to be dry when its $S_r > 0.5$.

Table 4. Soil state after drying to $s = 200$ kPa (Fig. 1, point C).

Cell (i)	1	2	3	4	5
Hard. par. p_0^*[kPa]	100	100	100	100	100
Suction [kPa]	30	100	180	200	200
Specific volume v_2^i	2.126	2.104	2.088	2.084	2.084
Precons. pres. p_0^i[kPa]	119.6	163.3	200.4	207.1	207.1

$$p_0^i = p_0(p_0^{*,i}, s^i) = p^c \left(\frac{p_0^{*,i}}{p^c} \right)^{\frac{\lambda(0)-\kappa}{\lambda(s^i)-\kappa}}, \quad i = 1..5 \qquad (6)$$

where $p_{\text{atm}} = 100$ kPa is atmospheric pressure. The average specific volume is, similarly to equation (4), given by:

$$v_2 = \frac{1}{n} \sum_{i=1}^{n} v_2^i = \frac{v_2^1 + v_2^2 + v_2^3 + v_2^4 + v_2^5}{5} = 2.097 \qquad (7)$$

After drying, the soil is isotropically loaded to p = 500 kPa (Fig 1, C–D). This final value of mean net stress is higher than the value of the preconsolidation pressure p_0^5 given in Table 4, so all the cells will be at stress states on the yield locus. The evolution of elastic and elasto-plastic loading is given in Table 5. The soil state after loading to 500 kPa is given in Table 6. Note that after loading the cell hardening parameters are different,

$$p_0^{*,1} > p_0^{*,2} > p_0^{*,3} > p_0^{*,4} = p_0^{*,5},$$

whereas the preconsolidation pressure p_0 is the same for each cell. This is because the values of suction are different for cells 1, 2, 3 and 4.

As the cells do not start yielding at the same mean net stress (compare Table 5) the transition between elastic and elasto-plastic regime appears smoother than in the original BBM. The greater the number of cells used in the model, the smoother the transition.

The value of hardening parameters $p_0^{*,i}$ and specific volumes v_3^i in Table 6 are calculated using:

$$p_0^{*,i} = p^c \left(\frac{p_0^i}{p^c} \right)^{\frac{\lambda(s^i)-\kappa}{\lambda(0)-\kappa}}, \quad i = 1..5 \qquad (8)$$

Table 5. Evolution of hardening during loading.

Loading					
Cell (i)	1	2	3	4	5
$p < p_0^1$	e	e	e	e	e
$p_0^1 < p < p_0^2$	ep	e	e	e	e
$p_0^2 < p < p_0^3$	ep	ep	e	e	e
$p_0^3 < p < p_0^4$	ep	ep	ep	e	e
$p > p_0^4 = p_0^5$	ep	ep	ep	ep	ep

e–elastic; ep–elasto-plastic.

Table 6. Soil state at $p = 500$ kPa (Fig. 1, point D).

Cell (i)	1	2	3	4	5
Hard. par. $p_0^{*,i}$[kPa]	377.3	253.6	202.6	195.4	195.4
Suction [kPa]	30	100	180	200	200
Specific volume v_3^i	1.855	1.906	1.929	1.932	1.932
Precons. pres. p_0[kPa]	500	500	500	500	500

$$v_3^i = N(0) - \lambda(s^i)\ln\frac{p_0}{p^c} - \kappa_s \ln\frac{s^i + p_{\text{atm}}}{p_{\text{atm}}}, \quad i = 1..5 \tag{9}$$

The average specific volume is:

$$v_3 = \frac{1}{n}\sum_{i=1}^{n} v_3^i = \frac{v_3^1 + v_3^2 + v_3^3 + v_3^4 + v_3^5}{5} = 1.911 \tag{10}$$

In the next stage, the soil is unloaded until it reaches the mean stress of 100 kPa (Fig. 1, D-E). The specific volume for each cell is then:

$$v_4^i = v_3^i - \kappa \ln\frac{p}{p_0}, \quad i = 1..5 \tag{11}$$

The average specific volume is calculated similarly as before (see e.g. 4).

At this stage the sample is wetted until fully saturated (Fig 1, E–F). The evolution of suction during wetting is given in Table 7 and the soil state after wetting is identified in Table 8. After saturation, the hardening parameters are unchanged and the value of preconsolidation pressure in each cell is equal to the value of hardening parameter in this cell.

The specific volume in Table 8 is calculated as

$$v_5^i = v_4^i + \kappa_s \ln\frac{p + p_{atm}}{p_{atm}}, \quad i = 1..5 \tag{12}$$

Table 7. Evolution of suction during wetting [kPa].

Loading					
Cell (i)	1	2	3	4	5
$S_r = 0.47$	30	100	180	200	200
$S_r < 0.5$	30	100	180	$s(S_r)$	$s(S_r)$
$S_r = 0.5$	30	100	180	180	180
$0.5 < S_r < 0.7$	30	100	$s(S_r)$	$s(S_r)$	$s(S_r)$
$Sr = 0.7$	30	100	100	100	100
$0.7 < Sr < 0.9$	30	$s(S_r)$	$s(S_r)$	$s(S_r)$	$s(S_r)$
$S_r = 0.9$	30	30	30	30	30
$S_r > 0.9$	$s(S_r)$	$s(S_r)$	$s(S_r)$	$s(S_r)$	$s(S_r)$

e—elastic; ep—elasto-plastic.

Table 8. Soil state after wetting ($s = 0$ kPa) (Fig. 1, point F).

Cell (i)	1	2	3	4	5
Hard. par. $p_0^{*,i}$[kPa]	377.3	253.6	202.6	195.4	195.4
Suction [kPa]	0	0	0	0	0
Specific volume v_5^i	1.900	1.972	2.012	2.019	2.019
Precons. pres. p_0^i[kPa]	377.3	253.6	202.6	195.4	195.4

Table 9. Evolution of hardening during loading.

Loading					
Cell (i)	1	2	3	4	5
$p < p_0^{*,1}$	e	e	e	e	e
$p_0^{*,1} < p < p_0^{*,2}$	ep	e	e	e	e
$p_0^{*,2} < p < p_0^{*,3}$	ep	ep	e	e	e
$p_0^{*,3} < p < p_0^{*,4}$	ep	ep	ep	e	e
$p > p_0^{*,4} = p_0^{*,5}$	ep	ep	ep	ep	ep

e—elastic; ep—elasto-plastic.

Table 10. Soil state at $p = 500$ kPa (final, Fig. 1, point G).

Cell (i)	1	2	3	4	5
Hard. par. p_0^*[kPa]	500	500	500	500	500
Suction [kPa]	0	0	0	0	0
Specific volume v_6^i	1.818	1.818	1.818	1.818	1.818
Precons. pres. p_0[kPa]	500	500	500	500	500

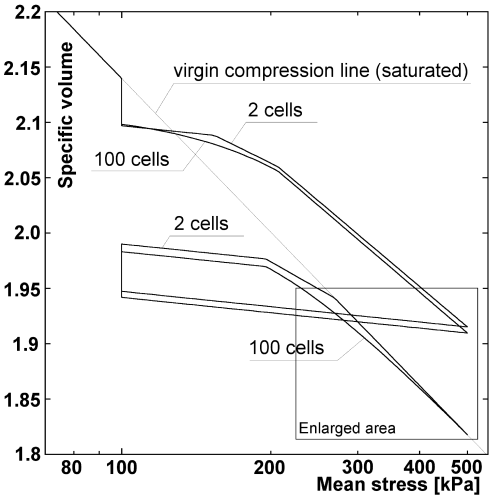

Figure 4. Influence of number of cells used in simulation—comparison between simulation with 2 and 100 cells.

The average specific volume is the mean of the specific volumes of calculated in each cell (see eq. 4).

Finally, the soil is loaded until the mean net stress p reaches a value of 500 kPa (Fig. 1, F–G). The loading is initially elastic, but as the mean stress increases, so the cells yield. The evolution of hardening during this loading is given in Table 9, and the final soil state is given in Table 10.

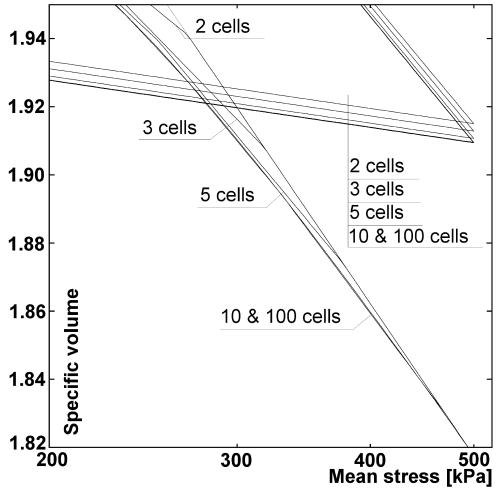

Figure 5. Influence of number of cells used in simulation—enlarged detail from Figure 4. Comparison between simulations using 2, 3, 5, 10 and 100 cells.

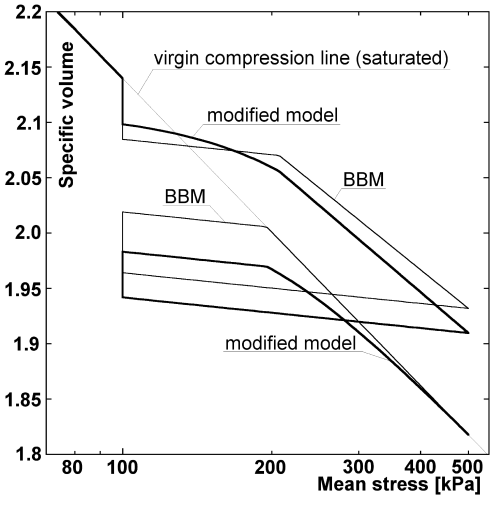

Figure 6. Comparison of the modified BBM with the original formulation.

The value of specific volume for each cell is then calculated as in (3) and the average specific volume as in (3). Note that the plastic behaviour will start gradually, with some yielding of the material before reaching the virgin compression line. This gradual transition will be better approximated when more cells are used. The influence of the number of cells used is illustrated in Figures 4 and 5.

6 COMPARISON WITH THE ORIGINAL BBM

The comparison has been made using a problem given in section 5. All the parameters used for the BBM were the same as in the previous example. The test began with a mean net stress $p = 10$ kPa on a saturated virgin compressed soil and the water retention curve is as depicted in Figure 2.

The comparison of the modified model prediction with the original BBM prediction (Fig. 6) reveals the differences. The slopes of the unsaturated compression lines are slightly different. This is to be expected, as the modified model effectively averages the specific volume and a range of suctions are operating within the material, whereas the original BBM uses only the current value of suction. The model can be calibrated, however, such that the fully yielded behaviour is similar. The other noticeable difference is the amount of elastic shrinking and swelling predicted by the models. This occurs because in the original formulation the shrinking depends on the final value of suction whereas in the modified form it is averaged over different changes in suction across the cells. As the shrinking and swelling behaviour are different, and the slope of the unsaturated compression line $\lambda(s)$ is steeper in the case of the modified model, the amount of collapse predicted by the original model is larger.

Finally, it is evident that the modified model predicts a smoother transition between the elastic and elasto-plastic regions. This smooth transition occurs also in the case of loading a fully saturated soil when it has previously been in an unsaturated state and was loaded beyond the yield point (of any of cells).

7 CONCLUSIONS

The proposed modifications to the BBM improve the capabilities of the model by offering more realistic material behaviour during yielding. The number of parameters in the model is unchanged as the water retention curve is also a pre-requisite for the BBM. On the other hand, the proposed solution may be just regarded as a convenient 'fix' to the model, as it does not work for the particular case of a saturated soil.

The calibration of the model requires some care, as calculations of the slope of the unsaturated compression line slope $\lambda(s)$ and amount of elastic shrinking/swelling is not so straightforward. The calibration process could employ an optimisation algorithm which would allow for automation of the process. Alternatively, the model parameters may be computed in a series of approximations. The latter approach would require an algorithm that would calculate deformations under given loading. It should be pointed out that the calibration of the model still does not require a greater

number of tests than those required for the BBM. This is certainly an advantage over a model that would introduce a bounding surface plasticity framework into the BBM.

The amount of computer resources required is higher than for the BBM. However, on current machines, it is entirely feasible to perform 2D Finite Element simulations with more than 10^5 elements using the enhanced model. Given that the speed (and memory) of computers continues to increase, it is very likely that in few years 3D analyses will be almost as quick as current 2D simulations.

It is worth adding that the algorithm complexity of this enhanced model is not significantly increased compared with the original BBM, as much of the code used for each of the cells is the same.

The proposed modified model is in the process of being validated against a wide range of experimental data. Only then can the improvements in prediction of unsaturated soil behaviour given by the modified model can be truly assessed.

ACKNOWLEDGMENTS

The authors gratefully acknowledge funding by the European Commission through the MUSE Research Training Network, contract: MRTN-CT-2004-506861. The authors would like to also thank the reviewer for valuable comments and insights.

REFERENCES

Alonso, E.E., Gens, A., Josa, A. 1990. A constitutive model for partially saturated soils. Géotechnique 40(3): 405–430.

Alonso, E.E., Gens, A., Josa, A., Hight, D.W. 1987. Special problems soils. General Reports. In proceedings of the 9th European Conference on Soil Mechanics and Foundation Engineering. Dublin. 3: 1087–1146.

Gallipoli, D., Wheeler, S.J., Karstunen, M. 2003. Modelling the variation of degree of saturation in a deformable unsaturated soil. Géotechnique 53(1): 105–112.

Gens, A., Alonso, E.E. 1992. A framework for the behaviour of unsaturated expansive clays. Can. Getech. J. 29: 1013–1032.

Houlsby, G.T. 1997. The work input to an unsaturated granular material. Géotechnique 47(1): 193–196.

Monroy, R. 2005. The influence of load and suction changes on the volumetric behaviour of compacted London Clay. PhD thesis. Imperial College, London.

Russell, A.R., Khalili, N. 2005. A unified bounding surface plasticity model for unsaturated soils. Int. J. Numer. Anal. Meth. Geomech. 30: 181–212.